Renewable Energy xxx (2016) 1–13

Contents lists available at ScienceDirect

Renewable Energy

journal homepage: www.elsevier.com/locate/renene

Wave energy resource assessment for Red Sea

V.M. Aboobacker*, P.R. Shanas, M.A. Alsaafani, Alaa M.A. Albarakati

King Abdulaziz University, Faculty of Marine Sciences, P. O. Box 80207, Jeddah, 21589, Saudi Arabia

ARTICLE INFO

Article history:
Received 8 May 2016
Received in revised form
28 September 2016
Accepted 30 September 2016
Available online xxx

Keywords:
Renewable energy
Red Sea
Wind waves
Wave power
Ocean energy
Inter-annual variability

ABSTRACT

Accurate assessment of wave energy potential has not been done so far in the offshore and nearshore waters of the Red Sea. In this paper, we present an assessment of wave energy resources in the Red Sea using numerical modelling. The wave conditions are simulated for 1979 to 2010 using a third generation ocean wave model, WAVEWATCH-III by forcing with CFSR winds. The model results are validated against *in situ* measurements in the Red Sea. The simulated wave parameters are used to estimate the wave power in the Red Sea during the 32 years – a reasonable long-term period for accurate assessment. The estimated wave power has been analyzed on a monthly, seasonal and inter-annual basis. The results indicate robust spatial and seasonal variations in mean wave power. Detailed investigations on wave energy potential have been carried out at a number of coastal locations in the Red Sea that consists of the coasts of Saudi Arabia, Yemen, Egypt, Sudan and Eritrea. Inter-annual variability in the mean wave power is also analyzed and discussed.

1. Introduction

Most of the maritime countries are benefitted by the proximity to the ocean renewable energies, especially the ocean wave energy. The high demand in the energy sector and the shortage of the conventional energies lead to the search for renewable and sustainable energies. The utilization of renewable and sustainable energy not only yields to overcome the energy demand but also reduces the carbon emissions. Globally, the estimated wave energy resource is more than 2 TW [1], which has the potential to become commercially viable [2]. Prior to the exploitation of these energies, a reliable assessment of the wave energy potential should be performed.

Wave energy resource assessments have been carried out globally and regionally [3–21]. For instance, the wave energy potential in the South China Sea and the East China Sea was derived from altimeter data (Wan et al., 2015) [5] and using wave modelling [6]. The wave energy resource assessments were carried out along the east coast of Malaysia [7,8], off Korea [9], off western Europe [10–12], along the Italian coast [13], in the Black Sea [14], in the Baltic Sea [15], off Portugal [16], off Hawaii [17], off Scotland [18], in the western Indian Ocean [19], along the Indian coast [20], and in the Persian Gulf/Arabian Gulf [21].

Long-term wave data is necessary for the wave energy assessment to average out the oscillations due to variabilities. Obtaining long-term wave data is a difficult task in most part of the world ocean, and the assessments will be restricted to limited coastal locations where long-term data is available [22]. Satellite data can be an alternative source, although it has limitations in accuracy along the land-water interface. In recent years, third generation spectral wave models such as WAVEWATCH III, SWAN and WAM have been used to assess wave energy resources [8,13,23–25]. A well-calibrated model will be adequate to reproduce long-term wind-wave data on fine temporal and coarse resolutions.

Recent studies indicate that waves are moderately high in most part of the Red Sea [26]. The significant wave height in the deep waters of the Red Sea is typically around 2.0 m and a maximum of 4.5 m was observed in the central Red Sea. The reversing monsoons cause seasonal variability at large scale. The maximum wave heights in the Red Sea are due to the mountain gap wind jets occurred during summer, which blows across the width of the central Red Sea through the central region (between 18° and 20°N). The wave convergence in the central Red Sea is another notable phenomenon, which occurred during winter due to the convergence in the atmosphere [27]. In addition, the local breezes contribute some amount of wave energies along the eastern part of the Red Sea.

The Middle East countries such as Saudi Arabia are relying on conventional energy resources such as petroleum and natural gas. Assessment of alternative resources, especially in the renewable

* Corresponding author.
E-mail address: vmabacker@gmail.com (V.M. Aboobacker).

http://dx.doi.org/10.1016/j.renene.2016.09.073
0960-1481/

energy sector, will be beneficial to understand the available resources and to exploit whenever such requirement arises. In addition, it will help the economy of the region, considering the present drop-down in the oil market. Limited studies are available on the wind and wave characteristics of the region; however the wave energy potential has not been assessed yet. In this view, wave energy resource assessment has been carried out for the Red Sea, which is ultimately useful for the bounded regions such as the west coasts of Saudi Arabia and Yemen, Egypt, Sudan and Eritrea. The present study aims to assess the wave power in the Red Sea during 1979–2010 using numerical modelling of wind-waves. The wave parameters thus obtained are used to estimate the wave power in the Red Sea. Average values of wave power were calculated on a monthly, seasonal and annual basis to analyse the variations.

2. Area of study

Fig. 1a shows the study area. The domain covers the geographical area: 32°–44°E; 12°–30°N. The Red Sea is a narrow seawater body in the Indian Ocean, lying between Asia and Africa and has an area of approximately 438,000 km^2. It is about 2300 km long and 360 km wide at the widest part. The average depth is around 490 m and the maximum recorded depth in the central axis of the Red Sea is 2920 m, while a figure of 3040 m has been also reported [28]. In the south, the Red Sea connects to the ocean body through the Bab el Mandeb Strait and the Gulf of Aden. In the north, the Red Sea is leading to the Gulf of Suez and Gulf of Aqaba.

The two important seasons in the region are winter (Dec–Mar) and summer (Jun–Sep). The intermediate seasons are referred as post-winter (Apr–May) and post-summer (Oct–Nov). In winter, north northwest (NNW) wind prevails in the northern Red Sea, while south southeast (SSE) wind dominates in the southern Red Sea [27]. In summer, winds are consistently from the NNW throughout the Red Sea. The average wind speeds over the Red Sea are close to 10 m/s during both winter and summer. In addition to the seasonal reversal, the unusual Tokar Gap wind occurs across 18° N during Jul–Aug with speeds above 15 m/s.

Fig. 1b shows the coastal locations considered for site-specific analysis of mean wave power. The locations P1 and P2 are on the west coast of Yemen, P3 to P9 on the west coast of Saudi Arabia, P10 at the east coast of Egypt, P11 on the east coast of Sudan, P12 on the east coast of Eritrea. Even though these locations are in random consideration, they are representing the coastal part of the populated (or industrial) regions around the Red Sea. The depths at these locations range 20–50 m, however the Red Sea coasts are generally very steep and the grid size of 0.03° used in this study may not well represent the shallow depths close the coast. Hence, we used deep water formulations (Section 3.2) to calculate the wave power from the modelled wave parameters. Table 1 shows the geographical co-ordinates, water depths and distance from the coast of the locations P1 to P12. Depending upon the slope, some locations are very close

Table 1
Geographical co-ordinates, water depth and distance from coast for locations P1 to P12.

Locations	Geographical co-ordinates		Water depth (m)	Distance from coast (km)
	Longitude	Latitude		
P1	43.16	13.29	25.5	6.7
P2	42.8	14.75	21.9	15.5
P3	42	17.5	39.9	15.2
P4	40.05	20.1	22.4	13.1
P5	38.8	21.8	20.4	18.4
P6	38.7	23.1	39.7	8.7
P7	37	25.05	37.3	22.3
P8	36.4	26.27	36.0	1.9
P9	35.66	27.34	39.2	2.0
P10	34.32	26.11	49.3	3.3
P11	37.28	19.68	28.8	2.2
P12	42.81	13.07	20.1	8.2

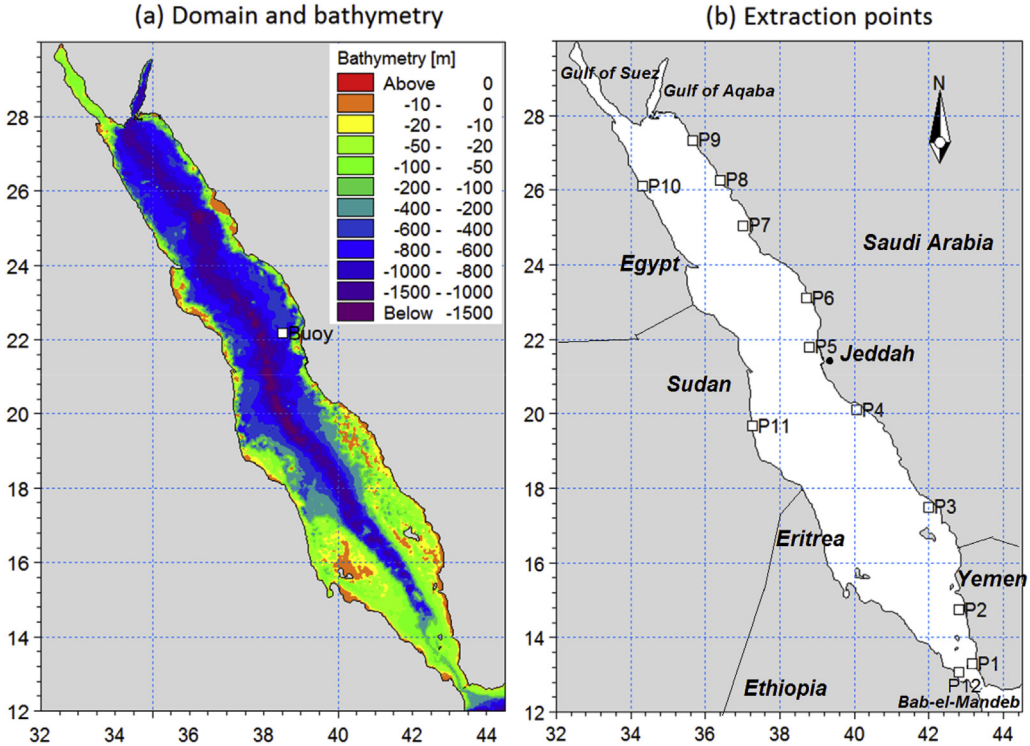

Fig. 1. (a) Domain and bathymetry covering the Red Sea. Met-Ocean buoy location is marked, (b) Selected coastal locations in the Red Sea (P1 to P12).

Please cite this article in press as: V.M. Aboobacker, et al., Wave energy resource assessment for Red Sea, Renewable Energy (2016), http://dx.doi.org/10.1016/j.renene.2016.09.073

to the coast and others are relatively far.

3. Numerical modelling

Numerical modelling has been carried out to hindcast the wind-waves in the Red Sea during 1979–2010 using WAVEWATCH III, version 4.18 (WW3 hereafter), a third generation spectral wave model developed at NOAA/NCEP (National Oceanic and Atmospheric Administration/National Centers for Environmental Prediction, USA) [29,30]. The model takes into account the growth, decay and transformation of multi-directional wave systems [31]. The model is based on the discrete spectral action balance equation, a generalization of the energy balance equation:

$$\frac{\partial N}{\partial t}+\frac{1}{\cos\phi}\frac{\partial}{\partial\phi}\dot{\phi}N\cos\theta+\frac{\partial}{\partial\lambda}\dot{\lambda}N+\frac{\partial}{\partial k}\dot{k}N+\frac{\partial}{\partial\theta}\dot{\theta}N=\frac{S}{\sigma} \quad (1)$$

Where θ is wave direction, ϕ - latitude, λ – longitude, k - wave number, the overdot represents the rate of change, and S is the net source of the spectrum which includes energy input by wind (S_{in}), a nonlinear wave-wave interaction term (S_{nl}), and dissipation due to white capping (S_{ds}) and bottom friction (S_{bt}). In addition, wave-bottom interactions (S_{bot}), depth-induced breaking (S_{db}), triad wave-wave interactions (S_{tr}) and scattering of waves by bottom features (S_{sc}) are also included specifically for the shallow waters. A finite difference scheme, with different time step sizes for time integration, spatial propagation, intra spectral propagation, and source term integration, is used to solve the action balance equation. A series of source term schemes such as ST2 ([32], ST3 ([33]), ST4 ([34]) and ST6 ([35]) are available in the model, however the scheme ST4 is found more reasonable in the Red Sea as evident from Langdon et al. [27].

The swell propagation from the Gulf of Aden to the Red Sea is almost negligible. This has been confirmed when we made several tests with varying wave parameters. This approach is also found in Langodan et al. [27]. Hence, zero energy flux is applied on the south boundary.

3.1. Model setup

The model domain and bathymetry are shown in Fig. 1. The spatial resolution of the rectangular grids is 0.03° × 0.03° (approx. 3.3 × 3.3 km) in longitude and latitude. Bathymetry data with 30 arc second resolution obtained from GEBCO [36] are interpolated to each element grids.

The wave model is forced using CFSR (Climate Forecast System Reanalysis, NOAA) winds during 1979–2010, a reasonably good long-term period for wave power assessment. The CFSR wind vectors (U and V components) are available for every 1 h at 0.312° × 0.312° spatial resolution. Recently, the accuracy of CFSR winds was evaluated worldwide [37–40]. For the sensitivity in using at the Red Sea, the CFSR winds have been validated with the ASCAT satellite winds, which are available daily at 0.25° × 0.25° spatial resolution. Both CFSR and ASCAT wind speeds were extracted at the buoy location during 2009. The comparison shows that the CFSR winds follow the pattern of ASCAT winds (Fig. 2a). At times, there are sharp peaks in the CFSR wind speed, during which the ASCAT wind speed follows a smooth curve. This difference is attributed to the coarse temporal resolution (daily) of the ASCAT winds. The scatter shows the accuracy of the comparison (Fig. 2b). It gives a correlation coefficient of 0.75 with a slight over-estimation (bias = 0.47 m/s) in the CFSR winds. The r.m.s error is 1.98 m/s (7.2%), and the scatter index is 0.33. We have also compared the CFSR winds with ASCAT winds at a few other locations in the Red Sea, which produces similar results.

The outputs of the model computations are the integral wave parameters such as significant wave height (H_s), energy wave period (T_e), mean wave period (T_m), peak wave period (T_p) and mean wave direction ($\bar{\theta}$), which are stored every 3 h. Here H_s and T_e are the two important parameters required for the calculation of wave power. Basically, the H_s and T_e are derived from the spectral moments as: $H_s = 4\sqrt{m_0}$, $T_e = m_{-1}/m_0$, where m_{-1} is the reciprocal of the first spectral moment (m_1) and m_0 is the zeroth moment.

The nth order spectral moment is defined as a function of frequency (f) and spectral energy density $S(f)$ as:

$$m_n = \int_0^\infty f^n S(f)df \quad (2)$$

3.2. Estimation of wave power

The wave energy flux per unit crest length (or wave power) for deep water locations is estimated using the formula:

$$P = \frac{\rho g^2}{64\pi}H_s^2 T_e \quad (3)$$

Here the unit of P is kW/m, H_s – the significant wave height (m), T_e- the energy wave period (s), ρ - the density of sea water (kg/m^3) and g - the acceleration due to gravity (m/s^2). Thus the wave power is directly proportional to the energy wave period and the square of the significant wave height.

3.3. Validation of model results

The wave model WW3 is widely used for hindcasting and forecasting of ocean waves by forcing with global re-analysis/forecast winds. Recently, the WW3 model was validated against measurements in the Indian Ocean [41]. The situation in the Red Sea is slightly different, where the influence of swells from the Indian Ocean is negligible, and the regional and local wind systems control the wave dynamics [27]. Hence we carried out validation of model results with wave parameters obtained from a met-ocean data buoy (23020) located at 22.162° N, 38.50° E, north of Jeddah, in the central Red Sea at a depth of 694 m (as marked in Fig. 1). The above data are freely available at the National Data Buoy Center (NDBC) website. The data consist of hourly significant wave height and mean wave period during Oct 2008–Dec 2010, and mean wave direction during 2010 and part of 2009. The validation of the model with the buoy is carried out for a complete year (2009) to cover all the months.

Fig. 3 shows the comparison between measured and modelled H_s and T_m during 2009. The time series comparison shows that the model H_s and T_m are very close to the measured H_s and T_m (Fig. 3a). The comparison is satisfactory at all ranges of H_s (lower and higher), while the model T_m is slightly over-estimated at higher mean wave periods. The scatter and statistics clearly indicate that the model results are in good agreement with the measured values (Fig. 3b). The correlation coefficients between the measured and modelled parameters are 0.91 and 0.75, respectively for H_s and T_m. The biases are 0.09 m for H_s and 0.42 s for T_m. The r.m.s. errors are well within the limits: 0.26 m (5.9%) and 0.85 s (9.5%), respectively for H_s and T_m. The scatter indices for H_s and T_m are 0.29 and 0.20, respectively. The measured mean wave direction is not sufficiently available for the year 2009; however the comparison (between measured and model) of mean wave directions during 2010 produces reasonably good agreement.

Please cite this article in press as: V.M. Aboobacker, et al., Wave energy resource assessment for Red Sea, Renewable Energy (2016), http://dx.doi.org/10.1016/j.renene.2016.09.073

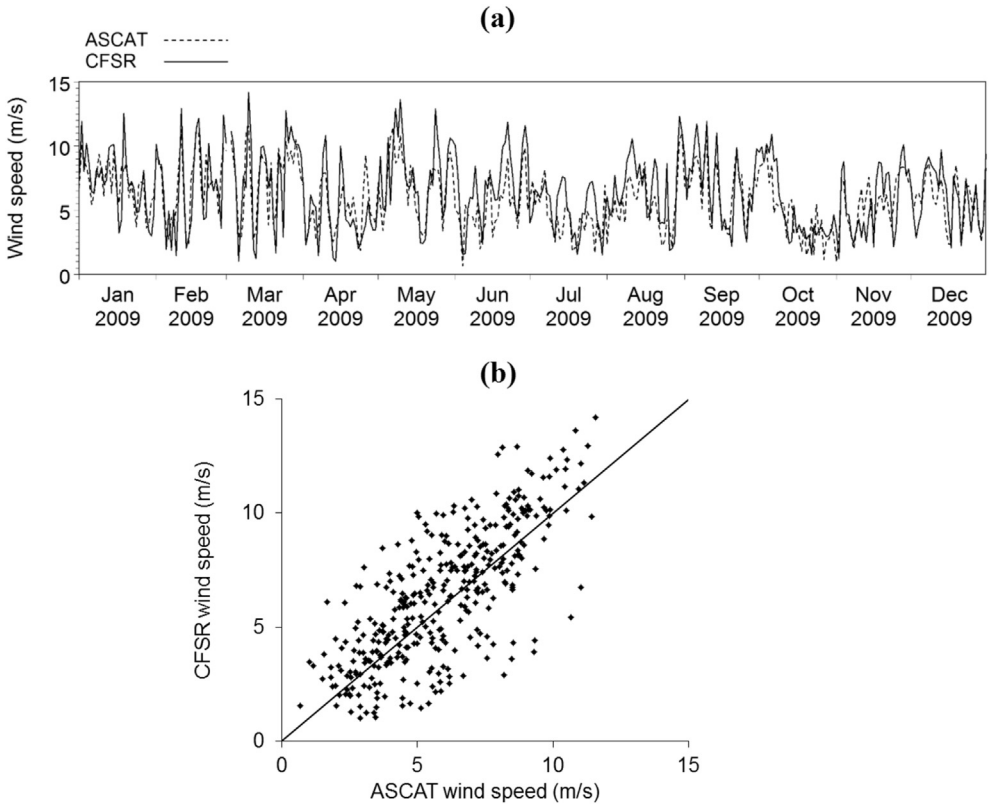

Fig. 2. (a) Time series comparison of ASCAT and CFSR wind speeds at buoy location during 2009, and (b) Scatter between ASCAT and CFSR wind speeds.

For the sensitivity of the model, the derived significant wave heights are compared with satellite altimeter wave heights at different locations in the Red Sea. The along-track mono-mission products of satellite altimeters Envisat, ERS-2, Jason-1 and Jason-2 are used for the comparison [42]. Table 2 shows the comparison of buoy data and model results with altimeter wave heights at buoy location, northern Red Sea (36.1° E, 25.4° N), central Red Sea (37.5° E, 22.3° N) and southern Red Sea (41.8° E, 15.7° N) during Oct 2008–Dec 2010. There is reasonable match for the significant wave heights among altimeters, buoy and the model. The correlation coefficients between the altimeters and buoy are 0.86–0.91 with r.m.s. errors of 0.22–0.39 m. Between the model and altimeter, the correlation coefficients are 0.78–0.93 considering all the above mentioned locations, where the bias is −0.06–0.2 m, r.m.s. error is 0.24–0.36 m, and the scatter index is 0.25–0.41.

4. Results and discussion

The wave power calculated for every 3 h was averaged for different months, seasons and years. The results are discussed in the following sections.

4.1. Long-term mean wave power

The long-term mean provides the average distribution of wave power eliminating the inconsistencies due to the variability. In this view, mean wave power has been estimated in the Red Sea from the time series wave power for the 32 years (1979–2010). Fig. 4a shows the spatial distribution of long-term mean wave power (kW/m) and standard deviation in the Red Sea. There is distinct amount of wave energy potential in the deep waters of the Red Sea, with the mean wave power ranges up to 4.5 kW/m. The highest mean wave power is obtained between 19° N and 21° N latitudes (in the central Red Sea), followed by at around 15° N latitude (in the southern Red Sea). The mean wave power is relatively low in the northern Red Sea, and very low in the two Gulfs (Gulf of Suez and Gulf of Aqaba), north of the Red Sea. The standard deviations are slightly above the magnitudes of mean wave power. These fluctuations are mainly due to the inter-annual variability caused by the climatic indices, and the variabilities are stronger (up to 5.0 kW/m standard deviation) in the central Red Sea, followed by the southern Red Sea.

Fig. 4b shows the annual mean wave power (kW/m) at selected locations in the Red Sea (P1 to P12), and the corresponding values are listed in Table 3. The mean wave power on the west coast of Yemen (P1 and P2) is 1.58–1.79 kW/m. The mean wave power at location P3 on the southern coast of Saudi Arabia in the Red Sea is low (0.34 kW/m), primarily due to the wave attenuation caused by a large number of coral reefs and islands along this coastal belt. This indicates that the nearshore regions of the southern coast of Saudi Arabia in the Red Sea are not well suitable for exploitation of wave energy on a large scale.

The central coast of Saudi Arabia in the Red Sea (P4 to P6) has a reasonable amount of wave energy, with the mean wave power ranges between 0.66 and 1.16 kW/m. The deep waters of the central Red Sea exhibit high wave power, almost double of that found near the coast. Among the locations of the northern coast of Saudi Arabia in the Red Sea (P7 to P9), the location P7 has the highest mean wave power (~1.5 kW/m) followed by P8 (~1 kW/m). The northernmost location (P9) off the coast of Saudi Arabia has relatively weak mean wave power (0.43 kW/m). The mean wave power at the representative locations for the western coasts of the Red Sea (P10 to P12) ranges between 0.51 and 1.03 kW/m. Unlike the eastern coasts, the shelf of the western coast is steep and the deep waters are reasonably close to the coast. Hence, higher mean wave power is

Please cite this article in press as: V.M. Aboobacker, et al., Wave energy resource assessment for Red Sea, Renewable Energy (2016), http://dx.doi.org/10.1016/j.renene.2016.09.073

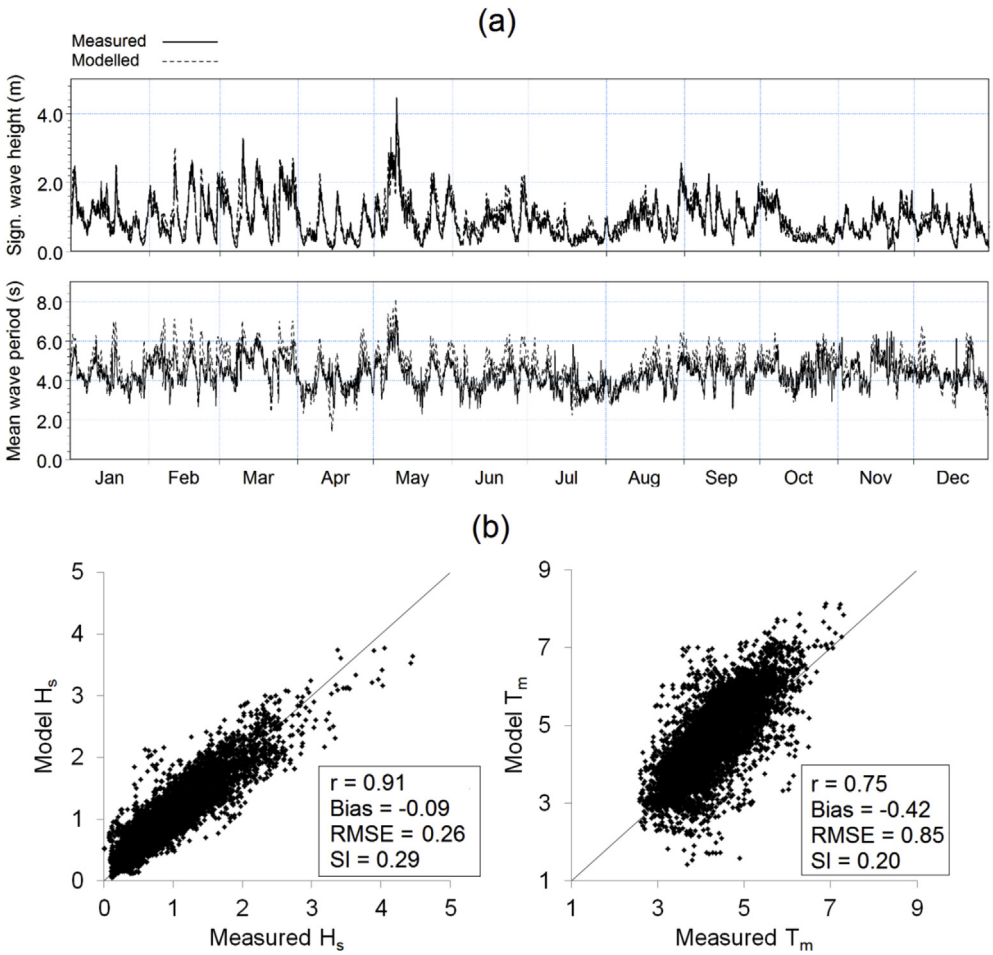

Fig. 3. Comparison between the measurements and model results: (a) Time-series of significant wave height and mean wave period during 2009 and (b) scatter of significant wave height and mean wave period.

Table 2
Error statics of significant wave heights: altimeter, model and buoy data.

Comparisons		Satellite	Error statistics			
			Correlation coefficient	Bias	RMSE	Scatter Index
Altimeter vs Buoy		ENVISAT	0.86	0.01	0.39	0.4
		ERS-2	0.91	−0.04	0.37	0.48
		JASON-1	0.9	0.02	0.22	0.25
		JASON-2	0.9	0.06	0.23	0.25
Altimeter vs Model	At buoy location	ENVISAT	0.87	0.04	0.36	0.35
		ERS-2	0.93	0.01	0.33	0.41
		JASON-1	0.88	0.05	0.24	0.25
		JASON-2	0.87	0.13	0.32	0.31
	Northern Red Sea	ENVISAT	0.85	0.04	0.3	0.29
		ERS-2	0.88	−0.01	0.28	0.26
		JASON-1	0.8	0.05	0.34	0.36
		JASON-2	0.78	−0.01	0.3	0.34
	Central Red Sea	ENVISAT	0.88	0.2	0.36	0.32
		ERS-2	0.92	0	0.34	0.29
		JASON-1	0.85	0.08	0.31	0.3
		JASON-2	0.82	0.14	0.35	0.33
	Southern Red Sea	ENVISAT	0.85	0.03	0.33	0.35
		ERS-2	–	–	–	–
		JASON-1	0.9	−0.02	0.26	0.29
		JASON-2	0.91	−0.06	0.26	0.26

expected within few kilometers from the coast.

Fig. 5 shows the rose of wave power during 1979–2010 at locations P1 to P12. The wave power below 0.1 kW/m are referred as calm, and thereby the waves at locations P3 and P9 are substantially calm. The WNW to NNE energy fluxes are dominated in most of the locations (P3 and P6 to P12), while ESE to S energy fluxes are

Please cite this article in press as: V.M. Aboobacker, et al., Wave energy resource assessment for Red Sea, Renewable Energy (2016), http://dx.doi.org/10.1016/j.renene.2016.09.073

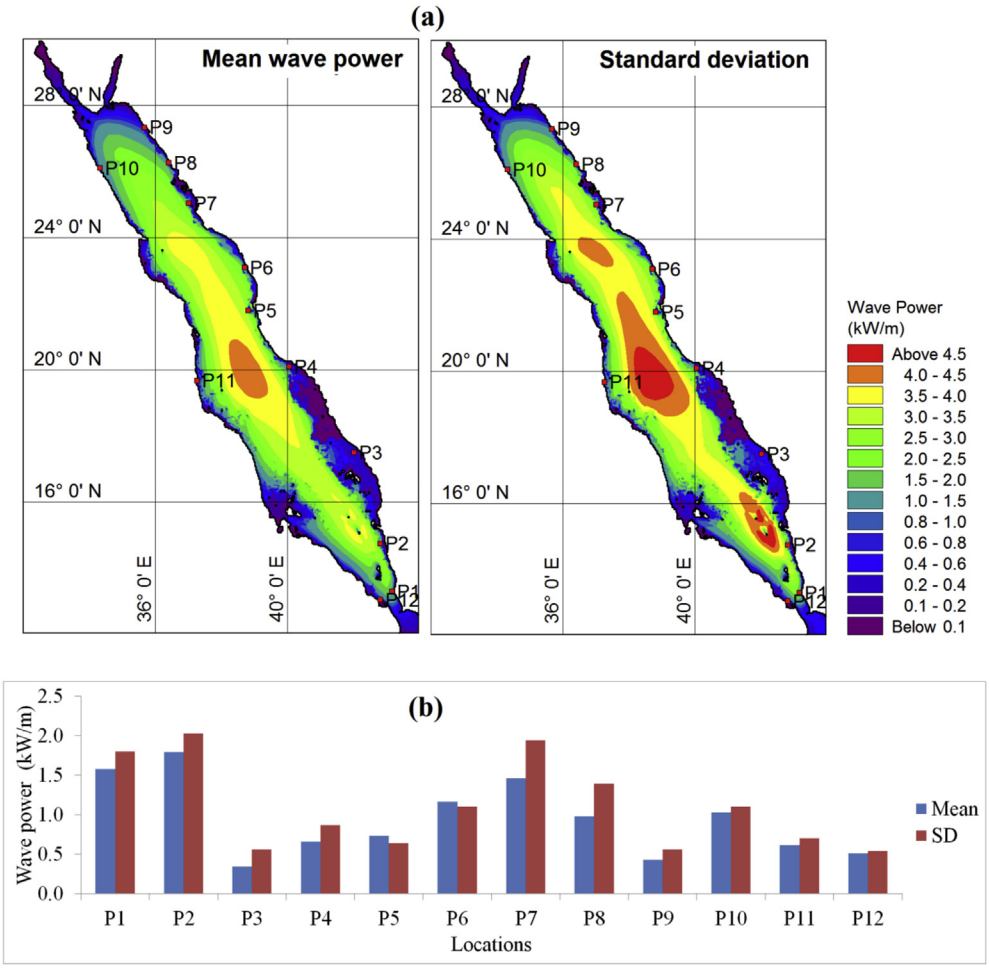

Fig. 4. (a) Spatial distribution of mean wave power (kW/m) and standard deviation in the Red Sea during 1979–2010, (b) mean wave power and standard deviation at locations P1 to P12 during 1979–2010.

Table 3
Annual mean wave power during 1979–2010 at locations P1 to P12.

Locations	Mean wave power (kW/m)				
	Annual	Winter	Post-winter	Summer	Post-summer
P1	1.58	2.84	1.42	0.33	1.73
P2	1.79	3.06	1.60	0.63	1.77
P3	0.34	0.41	0.25	0.39	0.21
P4	0.66	0.63	0.53	0.94	0.26
P5	0.74	0.80	0.77	0.81	0.43
P6	1.16	1.10	1.22	1.46	0.62
P7	1.46	1.45	1.60	1.69	0.89
P8	0.98	0.93	1.06	1.21	0.53
P9	0.43	0.41	0.47	0.54	0.23
P10	1.03	1.12	1.05	1.00	0.89
P11	0.62	0.98	0.61	0.34	0.45
P12	0.51	0.74	0.50	0.30	0.47

dominated at P1, P2, P4 and P5. Even though situated in the south, the wave power from SE is sheltered at P12 due to topographic features. In general, the seasonal reversal of the wind direction are significantly contributing to wave energy flux, mainly at locations P1, P2, P4, P5 and P6.

4.2. Seasonal mean wave power

The seasonal wave power is subject to the prevailing wind conditions over the region. Here the mean wave power during 4 seasons; winter, post-winter, summer and post-summer, are analyzed. Fig. 6 shows the seasonal mean wave power (kW/m) and standard deviation in the Red Sea during 1979–2010. The mean wave power is higher during winter, followed by the post-winter, summer and post-summer, respectively. The standard deviations of wave power are almost in the same magnitude or slightly higher, during all the seasons. The winter and post-winter standard deviations (up to 6.5 kW/m and 6.0 kW/m, respectively) were significantly contributed to the seasonal and inter-annual variability; their impacts are higher in the central and southern Red Sea. The winter and post-winter contribution to the inter-annual variability are also linked with the climatic indices such as ENSO and IOD (discussed in Section 4.4).

During winter, the highest mean wave power (6.0–6.5 kW/m) has been contained at two regions in deep water – around 19.5° N in the central Red Sea and around 15° N in the southern Red Sea. In general, the mean wave power in deep waters of the central and southern Red Sea is in the range 4.0–6.5 kW/m, while that in the northern Red Sea is between 1.5 and 4.5 kW/m. During post-winter, the highest mean wave power (4.5–5.0 kW/m) is at 20° N in the central Red Sea followed by at 23.5° N (4.0–4.5 kW/m) in the northern Red Sea, while that in the southern Red Sea is up to 3.0 kW/m.

During summer, the highest mean wave power is around 22.5° N (up to 4.5 kW/m). In general, the deep waters between 17° N and

Please cite this article in press as: V.M. Aboobacker, et al., Wave energy resource assessment for Red Sea, Renewable Energy (2016), http://dx.doi.org/10.1016/j.renene.2016.09.073

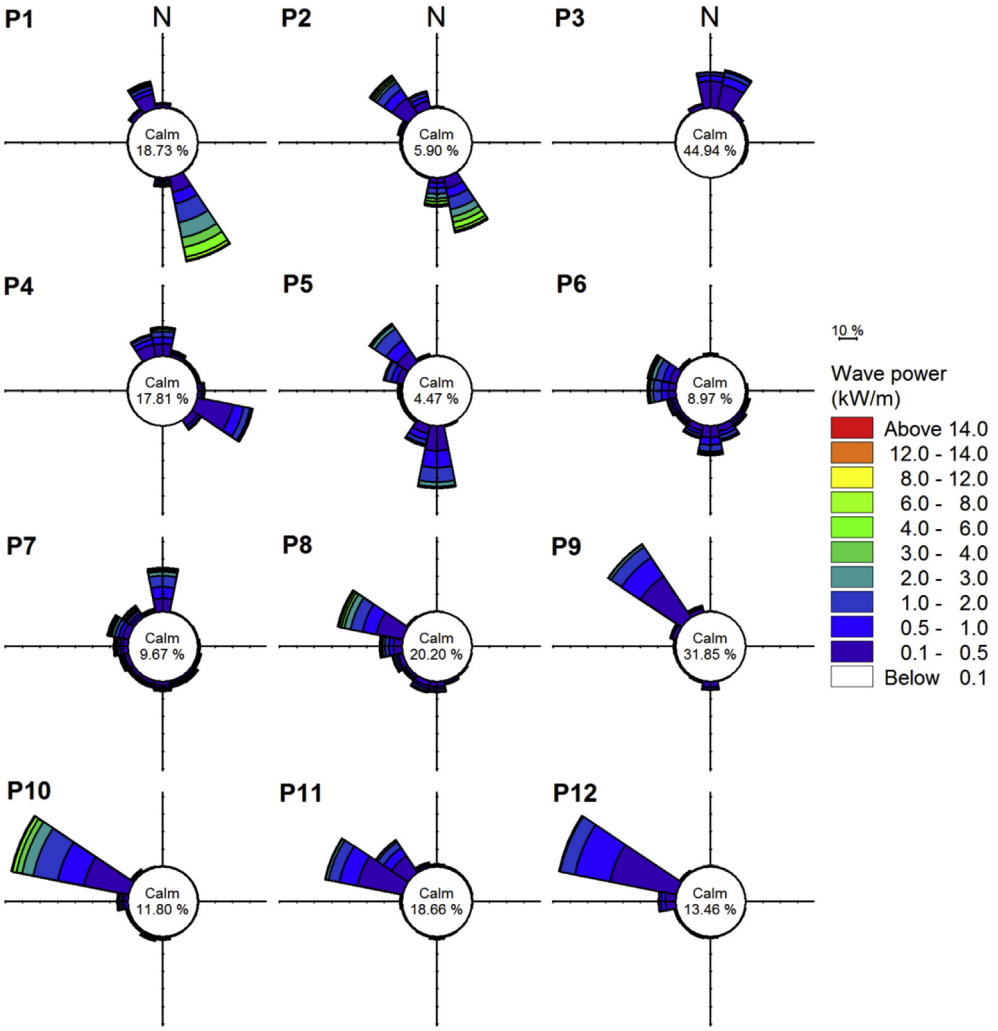

Fig. 5. Rose of wave power during 1979–2010 at locations P1 to P12.

26° N latitudes (central and northern Red Sea) have the mean wave power of the range 2.0–4.5 kW/m, while those in the southern Red Sea are below 2.5 kW/m. During post-summer, the wave power weakens in the northern and central Red Sea (below 3.0 kW/m), while the southern Red Sea exhibits relatively higher mean wave power (up to 4.5 kW/m).

The seasonal mean wave power at the coastal locations in the Red Sea has been analyzed. Fig. 7 shows the seasonal mean wave power at locations P1 to P12 during 1979–2010, and the corresponding values are listed in Table 3. The seasonal response of the wave power differs according to the locations., the highest mean wave power at locations P1 to P3 and P10 to P12 is during winter, while that at locations P4 to P9 is during summer. This indicates that the mean wave power during winter is stronger in the southern Red Sea and west coasts of Red Sea. The mean wave power during summer is stronger along the coasts of Saudi Arabia in the central and northern Red Sea. These observations are consistent with the earlier studies [26,27].

Along the west coast of Yemen (P1 and P2), the mean wave power during winter is 2.84–3.06 kW/m, followed by post-summer (1.73–1.77 kW/m), post-winter (1.42–1.60 kW/m) and summer (0.33–0.63 kW/m), respectively. Along the coast of Saudi Arabia in the southern Red Sea (P3), the mean wave power during winter is 0.41 kW/m, followed by summer (0.39 kW/m), post-winter (0.25 kW/m) and post-summer (0.21 kW/m), respectively. Along the coast of Saudi Arabia in the central Red Sea (P4 to P6), the mean wave power during summer is 0.81–1.46 kW/m, while that during winter, post-winter and post-summer are 0.63–1.10 kW/m, 0.53–1.22 kW/m and 0.26–0.62 kW/m, respectively. Along the coast of Saudi Arabia in the northern Red Sea (P7 to P9), the mean wave power during summer is 0.54–1.69 kW/m, followed by post-winter (0.47–1.60 kW/m), winter (0.41–1.45 kW/m) and post-summer (0.23–0.89 kW/m). Along the east coast of Egypt (P10), the mean wave power during winter is 1.12 kW/m, followed by post-winter (1.05 kW/m), summer (1.0 kW/m) and post-summer (0.89 kW/m), respectively. Along the coast of Sudan and Eritrea (P11 and P12), the mean wave power during winter is 0.74–0.98 kW/m, followed by post-winter (0.50–0.61 kW/m), post-summer (0.45–0.47 kW/m) and summer (0.30–0.34 kW/m), respectively.

4.3. Monthly mean wave power

Fig. 8 shows the monthly mean wave power in the Red Sea during 1979–2010. The highest mean wave power in the Red Sea is obtained during Dec–Mar (up to 6.5 kW/m), and the lowest is during Jul–Aug (up to 4.0 kW/m). During Jan and Feb, the highest mean wave power is in the central and the southern Red Sea, while

Please cite this article in press as: V.M. Aboobacker, et al., Wave energy resource assessment for Red Sea, Renewable Energy (2016), http://dx.doi.org/10.1016/j.renene.2016.09.073

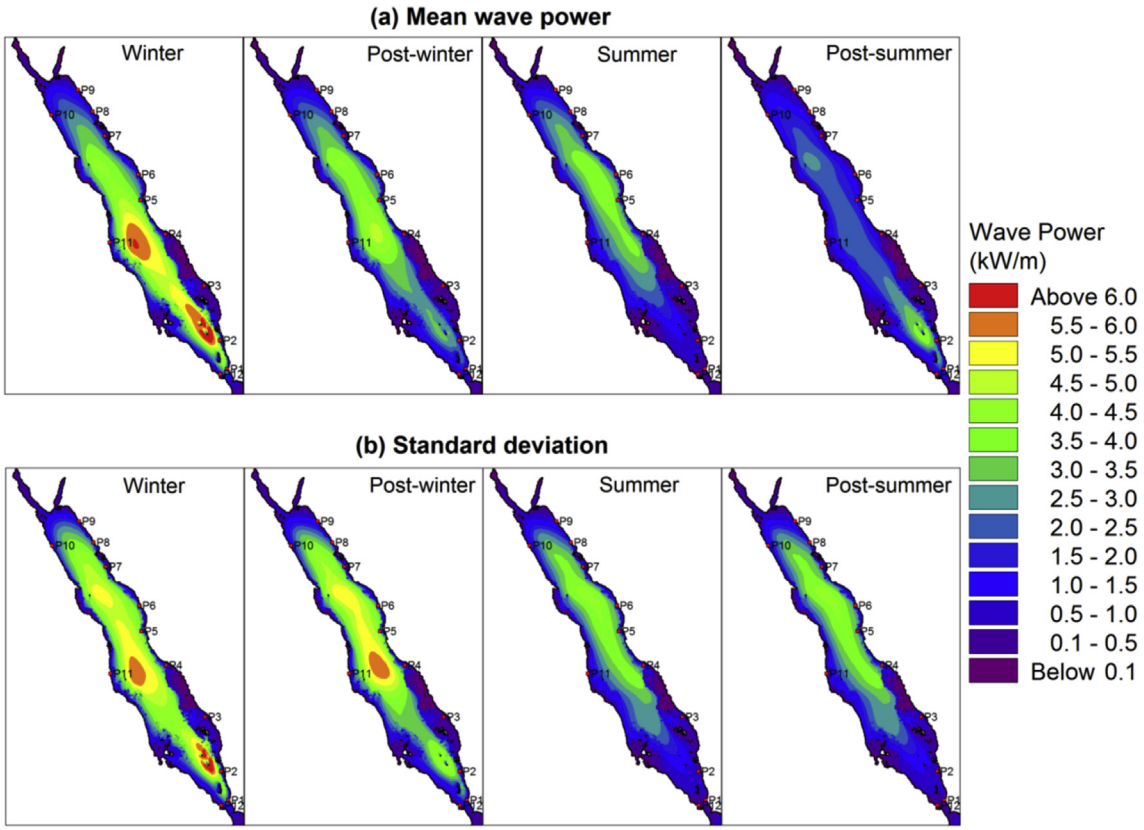

Fig. 6. Spatial distribution of (a) seasonal mean wave power (kW/m) and (b) standard deviation in the Red Sea during 1979–2010.

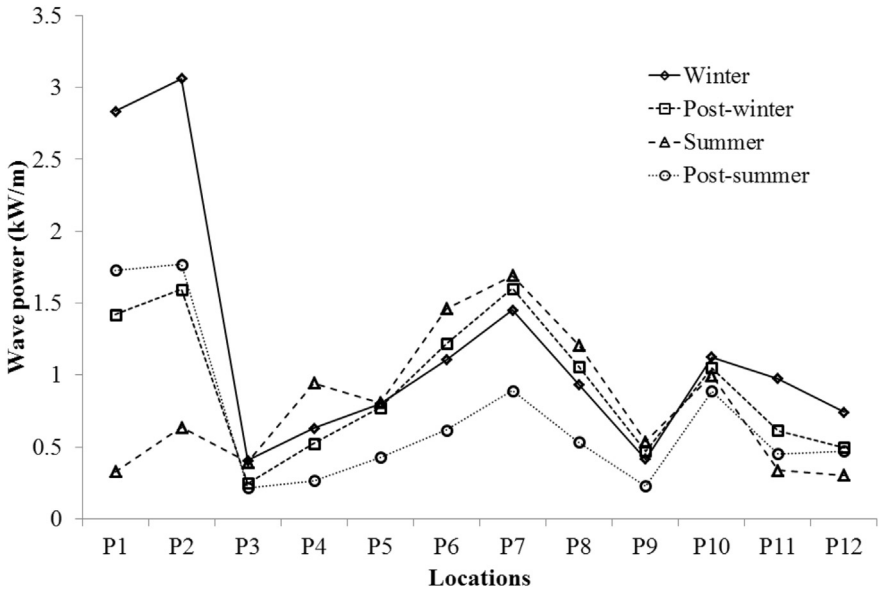

Fig. 7. Seasonal mean wave power (kW/m) at locations P1 to P12.

during Mar the mean wave power has been reduced in the southern Red Sea, but increased in the lower part of the northern Red Sea. During Apr and May, the wave power has been dropped considerably with the highest mean wave power (around 5.0 kW/m) observed in the central Red Sea. During Jun, a slight increase in mean wave power is found in the central and southern Red Sea, compared to Apr and May. During Jul and Aug, the wave power has been dropped significantly, even though two certain regions in the central Red Sea exhibit some peaks (up to 4.0 kW/m). One of these regions (around 18° N) is under the influence of Tokar Gap winds, especially during July (as marked in the figure). Similar observations were found around the Tokar wind influenced regions with a high wave energy propagation and strong gradients towards the east [26].

Please cite this article in press as: V.M. Aboobacker, et al., Wave energy resource assessment for Red Sea, Renewable Energy (2016), http://dx.doi.org/10.1016/j.renene.2016.09.073

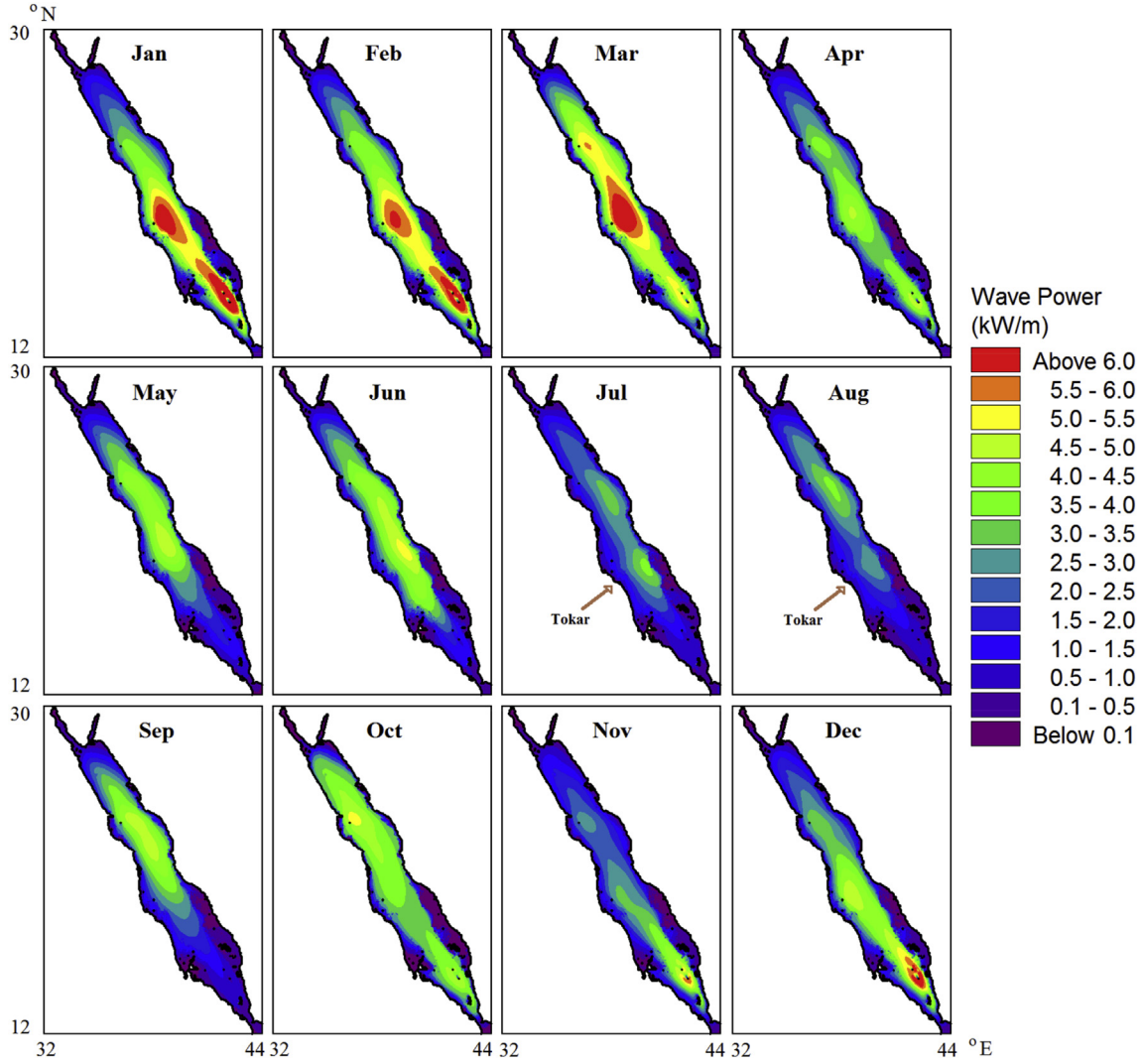

Fig. 8. Monthly mean wave power (kW/m) in the Red Sea during 1979–2010.

During Sep, the mean wave power in the southern Red Sea is very low (up to 1.5 kW/m), while the peaks are in the upper part of the central Red Sea (up to 5.0 kW/m). The mean wave power during Oct is reasonably higher throughout the Red Sea with a peak in the upper part of the central Red Sea (up to 5.5 kW/m). During Oct and Jan, smaller northeastern mountain gap wind jets (other than Tokar Gap wind jets) enhanced the wave energy along the northeast coast [26]. The months Nov and Dec exhibit a completely different pattern compared to the previous months, but with a rapid increase in mean wave power in the southern Red Sea; up to 6.0 kW/m and 6.5 kW/m during Nov and Dec, respectively. During Dec, a significant increase in wave power has been found in the central Red Sea.

Fig. 9 shows the monthly mean wave power at locations P1 to P12. At locations P1 and P2, the highest mean wave power is during Jan (3.1 kW/m and 3.4 kW/m, respectively at P1 and P2) and Feb (same values as in Jan), followed by Dec (2.7 kW/m and 3.0 kW/m, respectively at P1 and P2). Earlier studies ([26] and [27]) also described that the regions north of Bab-el-Mandeb (southern Red Sea) has consistently larger wave heights during the winter months. The lowest mean wave power at these locations is during Aug (0.24 kW/m and 0.51 kW/m, respectively at P1 and P2). The mean wave power at P3 is considerably low in all the months; with the maximum in Jul (0.54 kW/m).

The mean wave power at P4 and P5 follows the same pattern in all the months. The highest mean wave power at P4 is during Jul (1.2 kW/m) followed by Jun (1.1 kW/m), while that at P5 is during Jul (1.0 kW/m) followed by Mar (0.94 kW/m). The lowest mean wave power is during Oct; 0.21 kW/m and 0.42 kW/m, respectively at P4 and P5. The mean wave power at P6 and P7 follows the same patterns in all the months. The highest mean wave power at P6 is during Jun and Sep (1.7 kW/m and 1.6 kW/m, respectively), while that at P7 is during Mar and Sep (2.0 kW/m and 1.95 kW/m, respectively). The lowest mean wave power at these locations is during Nov (0.56 kW/m and 0.82 kW/m, respectively at P6 and P7) consistent with the observations of Ralston et al. [26].

The mean wave power is fairly high at P8 and low at P9. The highest mean wave power at P8 is during Mar, Jun and Sep (~1.3 kW/m), and the lowest is during Nov (0.47 kW/m). The highest and lowest mean wave powers at P9 are during Jun (0.59 kW/m) and Nov (0.22 kW/m), respectively. The mean wave power at P10 is nearly consistent throughout the year, with the highest is during Mar (1.55 kW/m) and lowest is during Jul (0.81 kW/m). Even though the locations P11 and P12 are very far each other, the mean wave power follows the same pattern in all months. The highest mean wave power at P11 is during Jan (1.1 kW/m) followed by Mar (1.0 kW/m), while those at P12 is during Jan

Please cite this article in press as: V.M. Aboobacker, et al., Wave energy resource assessment for Red Sea, Renewable Energy (2016), http://dx.doi.org/10.1016/j.renene.2016.09.073

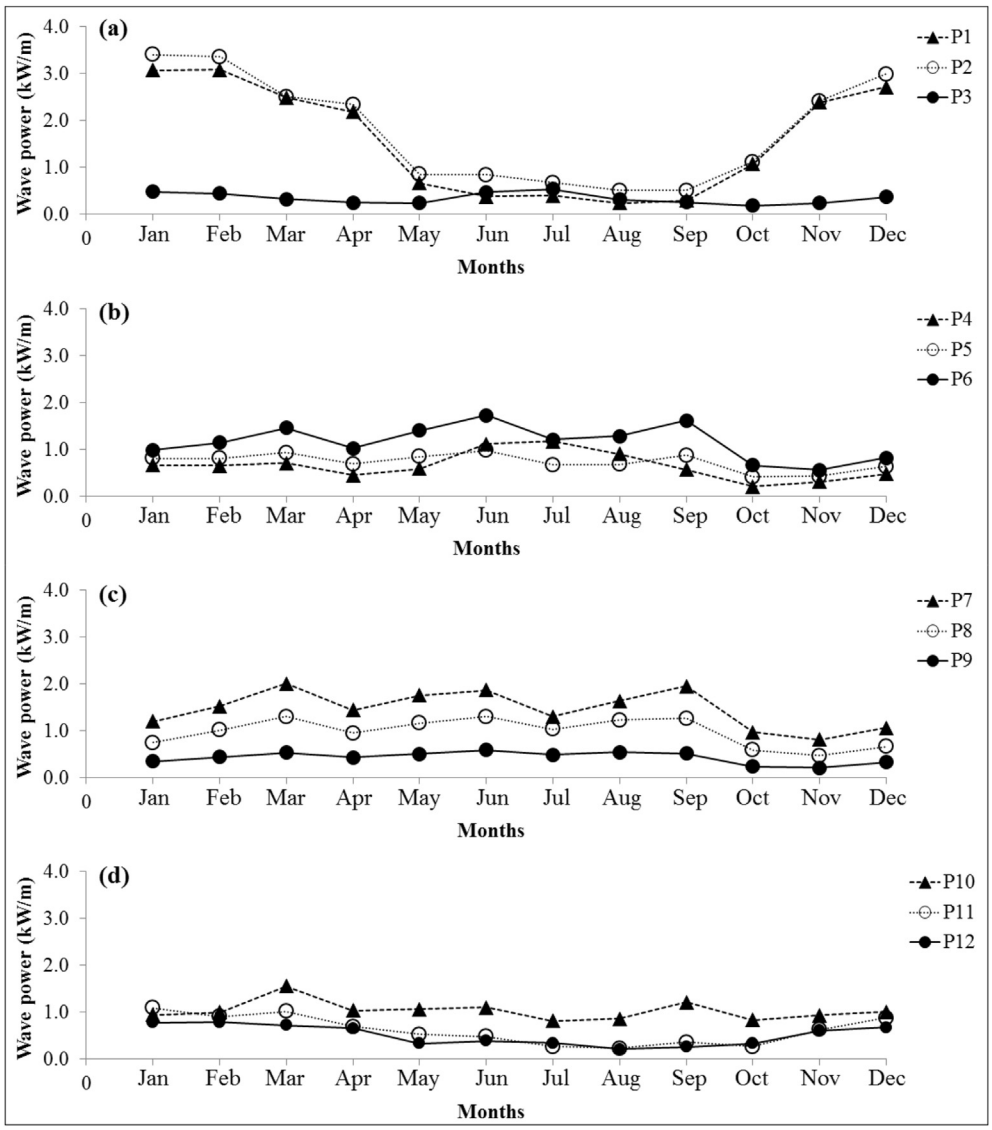

Fig. 9. Monthly mean wave power (kW/m) at locations P1 to P12.

and Feb (0.78 kW/m) followed by Mar (0.72 kW/m). The lowest mean wave power at these locations is during Aug (0.24 kW/m and 0.22 kW/m, respectively at P11 and P12).

It is remarkable that the mean wave power is higher along the west coast of Yemen (P1 and P2) during Nov–Apr, followed by the part of the west coast of Saudi Arabia between P6 and P7 consistently during Jan–Sep. The mean wave power is relatively weaker along the west coast of Yemen during May–Sep. In general, along the west coast of Saudi Arabia the weakest mean wave power is during Oct–Nov. Considering different wind systems prevailing over the region, mountain gap winds as well as the sea breezes in addition to the monsoonal winds plays a major role in maintaining the high temporal (for example, monthly and seasonal) and spatial variability of the wave power in the Red Sea.

4.4. Inter-annual variability in wave power

The year to year variations in the wave energy in the Indian Ocean is generally associated with the global oscillations such as ENSO (El-Niño Southern Oscillations) and IOD (Indian Ocean Dipole). However, such fluctuations may not be evident to full extent in the Red Sea, as the region is very small compared to the global oceans, and almost isolated from the ocean body. In this context, we have made an attempt to analyze the fluctuations in the annual mean wave power in the Red Sea. Globally, the winds are weaker during El Niño years and stronger during La Niña years, and hence, the wave energy should follow the same trend.

Fig. 10 shows the annual mean wave power during 1979–2010 at locations P1 to P12. Weak to strong El-Niño and La-Niña years were classified in the Oceanic Niño Index (ONI). Even though not so apparent, some glimpses of ENSO are visible in the annual mean wave power. For instance, the years 1983–1984, 1998–1999 and 1999–2000 were the La-Niña years during which the mean wave power shows an increase in the Red Sea, as evident from the locations P4 to P11. The locations P1 to P3 and P12 are in the southern part of the Red Sea, which responded neutrally to the 1998–1999 event and in opposite phase to the 1999–2000 and 1983–1984 events. In this perspective, it is important to note that the southern Red Sea not only neutral, at times they are in opposite phase with the La-Niña. We also find opposite phase in the southern Red Sea when the El-Niño occurs along with positive IODs (e.g., 1982–1983). This indicates that the IOD has an impact on the

Please cite this article in press as: V.M. Aboobacker, et al., Wave energy resource assessment for Red Sea, Renewable Energy (2016), http://dx.doi.org/10.1016/j.renene.2016.09.073

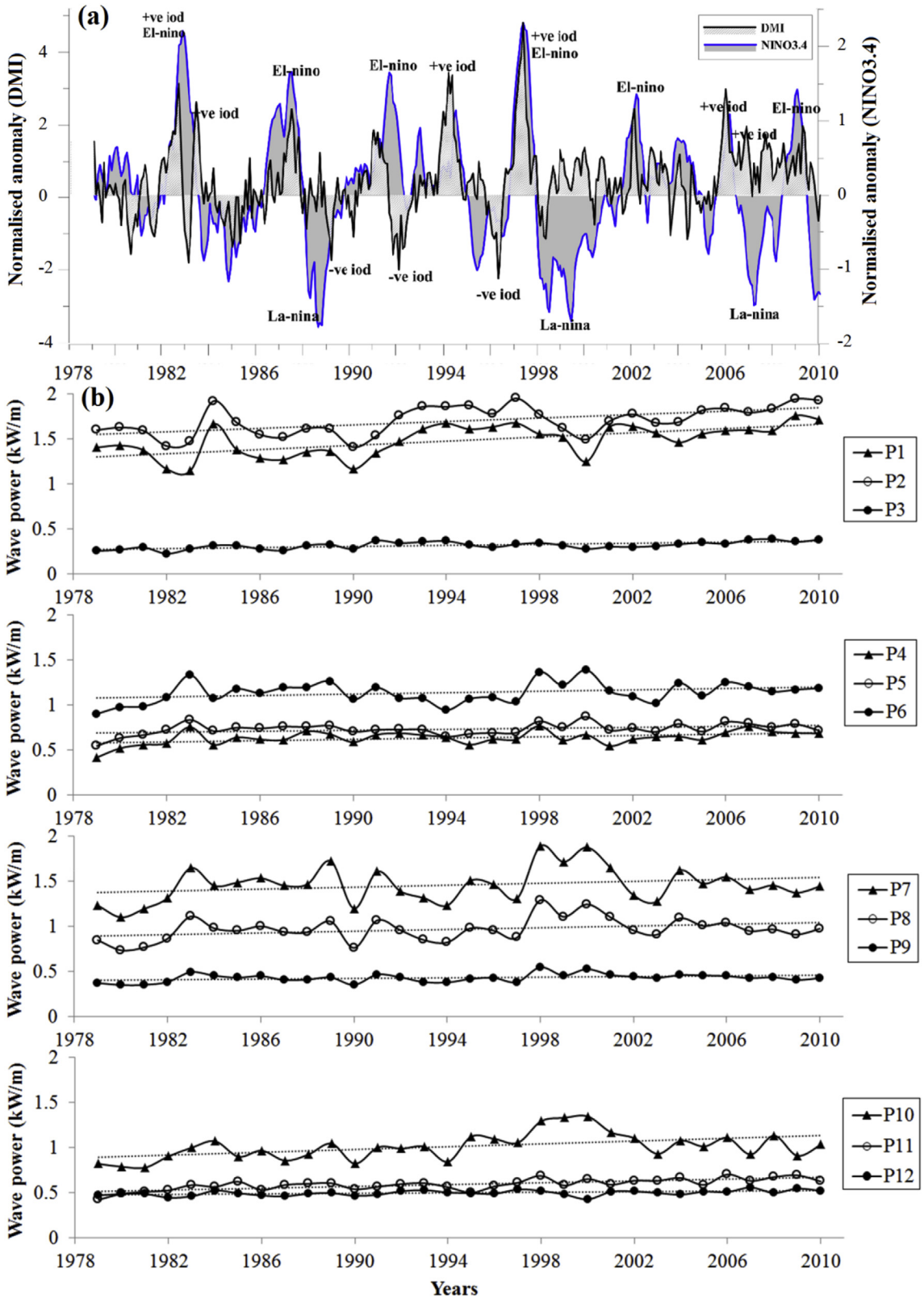

Fig. 10. Inter-annual variability of mean wave power (kW/m) at locations P1to P12 during 1979–2010: (a) Nino and DMI index (b) mean wave power and trends at P1 to P12.

southern Red Sea. Irrespective of the above two inferences, all the locations in the Red Sea (P1 to P12) follow the same pattern during 1990, which was neither an ENSO nor an IOD year, but the drop-down in wave power is yet to be understood. This leads to the observation that the whole Red Sea responds to the local met-ocean condition in similar patterns in the absence of global oscillations.

The linear trends of annual mean wave power at locations P1 to P12, accounting the temporal variability during 1979–2010, have

Please cite this article in press as: V.M. Aboobacker, et al., Wave energy resource assessment for Red Sea, Renewable Energy (2016), http://dx.doi.org/10.1016/j.renene.2016.09.073

Table 4
The variations in mean wave power during 1979–2010 at locations P1 to P12.

Locations	Increase in mean wave power (kW/m)		Annual % of increase
	1979–2010 (32 years)	Annual rate of increase	
P1	0.29	0.0092	0.60
P2	0.36	0.0112	0.93
P3	0.09	0.0027	0.87
P4	0.11	0.0036	0.63
P5	0.08	0.0025	0.41
P6	0.12	0.0039	0.37
P7	0.17	0.0052	0.37
P8	0.15	0.0046	0.50
P9	0.05	0.0016	0.48
P10	0.24	0.0075	0.79
P11	0.16	0.0048	0.91
P12	0.05	0.0015	0.30

been estimated (Fig. 10). The trend lines indicate that the trends are positive at all the locations (P1 to P12). A similar trend has been observed for the spatially averaged mean wave power. This indicates that there is a gradual increase in wave power in the whole Red Sea due to the increase in wave height, which can be attributed to the changes in global climate. Table 4 shows the variations in mean wave power and the annual rates at locations P1 to P12. It varies from 0.05 to 0.36 m per 32 years (or 0.0015–0.0112 m annually) according to the magnitude of the incident waves at each location. The most reasonable approach is the quantification of the increments in terms of percentages. The annual percentage increase of mean wave power in the Red Sea is between 0.3% and 0.93% with an average value of around 0.6%. The highest increase (>0.8%) is at locations P2, P3 and P11, while the lowest (<0.4%) is at P6, P7 and P12. In general, higher wave power is expected along the coasts of Red Sea in the future. Even though any of the global studies are not precisely covered the Red Sea, the trends in the Indian Ocean (especially in the Arabian Sea) are generally positive ([43,44]). The IPCC also projects an increasing trend in extreme wave heights in mid-latitudes ([45]).

5. Summary and conclusions

The wave energy resource assessment was carried out for the Red Sea considering the wave conditions over a long-term period, 1979–2010. The wave parameters in the Red Sea were derived using WW3, a third generation wave model by forcing with CFSR winds, and validated against available in-situ measurements in the central Red Sea. The comparison between the measurements and model results provides the correlation coefficients of 0.91 and 0.75, and the r.m.s. errors of 0.26 m (5.9%) and 0.85 s (9.5%) for the significant wave height and mean wave period, respectively.

The wave power was computed using the hindcasted wave parameters over the 32 years, and estimated the monthly, seasonal and annual mean wave powers. The long-term mean over 32 years indicates that the deep waters of the Red Sea have a distinct amount of wave power, ranges up to 4.5 kW/m, with the highest mean wave power in the central Red Sea. Seasonally, winter prevails for the higher wave power (up to 6.5 kW/m) followed by post-winter (up to 5.0 kW/m), summer and post-summer (up to 4.5 kW/m). A notable feature is the spatial variations of highest mean wave power between the seasons; during winter in the central and southern Red Sea, during post-winter in the central Red Sea, during summer in the central Red Sea and lower part of the northern Red Sea, and during post-summer in the southern Red Sea. On monthly classification, the highest mean wave power in the Red Sea is during Dec–Mar (up to 6.5 kW/m), and the lowest is during Jul–Aug (up to 4.0 kW/m). Even though relatively low, the lower part of the central Red Sea is characterized by the wave power generated due to the winds from Tokar gap.

The mean wave power at selected coastal locations (P1 to P12) was estimated and analyzed. The highest long-term mean wave power is along the west coast of Yemen (up to 1.8 kW/m), followed by the central west coast of Saudi Arabia (up to 1.6 kW/m) and the east coast of Egypt (up to 1.03 kW/m). Seasonally, the winter has the highest mean wave power along the coasts of Yemen (up to 3.1 kW/m), Egypt (1.12 kW/m), Sudan (up to 1.0 kW/m) and Eritrea (0.74 kW/m), while summer has the highest mean wave power along the coast of Saudi Arabia (up to 1.7 kW/m in the central region). In all the seasons, the southern part of the coast of Saudi Arabia responds with low mean wave power (up to 0.41 kW/m). On monthly classification, the mean wave power is higher along the west coast of Yemen during Nov–Apr and relatively weaker during May–Sep, while that along the west coast of Saudi Arabia is almost higher and consistent during Jan–Sep and weaker during Oct–Nov. Along the east coast of Egypt, the mean wave power is higher during Mar, while slightly low in all other months. Along the coasts of Sudan and Eritrea, the highest mean wave power is during Nov–Apr. Considering different wind systems prevailing over the Red Sea, mountain gap winds and the sea breezes play major roles in maintaining high temporal and spatial variability of the wave power in the Red Sea.

Inter-annual variability and trends of mean wave power during 1979–2010 were analyzed at selected coastal locations (P1 to P12). The trends are positive at all the locations with an average increase of mean wave power by 20% during the 32 year period. The ENSO and IOD have a distinct role in the variability of mean wave power in the Red Sea. Under neutral conditions (non-ENSO non-IOD years), the pattern of annual mean wave power is similar at all the locations in the Red Sea, while under ENSO or IOD conditions the southern Red Sea responds in opposite or neutral to the pattern present at the rest of the Red Sea.

Even though brief, the present investigation on the wave energy potential and the associated characteristics such as inter-annual variability and long-term trends in the Red Sea highlights the quantification of wave power and the suitability of the exploration of the renewable energy in relevant areas. It will also help the developers and the operators of the Wave Energy Convertors (WEC) in decision making.

Acknowledgements

The author thanks King Abdulaziz University (KAU), Jeddah for providing necessary facilities to carry out the research. The second author, Mr. Shanas P.R. is grateful to the Deanship of Graduate Studies, King Abdulaziz University for providing Ph.D. Fellowship.

Please cite this article in press as: V.M. Aboobacker, et al., Wave energy resource assessment for Red Sea, Renewable Energy (2016), http://dx.doi.org/10.1016/j.renene.2016.09.073

The simulations in this work were performed at King Abdulaziz University's High Performance Computing Center (Aziz Supercomputer) (http://hpc.kau.edu.sa).

References

[1] K. Gunn, C. Stock-Williams, Quantifying the global wave power resource, Renew. Energy 44 (2012) 296–304.
[2] P. Clement, A. McCullen, A. Falcao, F. Fiorentino, Gardner Hammarlund K. Wave energy in Europe: current status and perspectives, Renew. Sust. Energy Rev. 6 (5) (2002) 405–431.
[3] R.A. Arinaga, K.F. Cheung, Atlas of global wave energy from 10 years of reanalysis and hindcast data, Renew. Energy 39 (1) (2012) 49–64.
[4] Zheng Chongwei, Shao Longtan, Shi Wenli, Su Qin, Lin Gang, Li Xunqiang, An assessment of global ocean wave energy resources over the last 45 a, Acta Oceanol. Sin. 33 (1) (2014) 92–101.
[5] Y. Wan, J. Zhang, J. Meng, J. Wang, A wave energy resource assessment in the China's seas based on multi-satellite merged radar altimeter data, Acta Oceanol. Sin. 34 (3) (2015) 115–124.
[6] Zheng Chongwei, Zhuang Hui, Li Xin, Li Xunqiang, Wind energy and wave energy resources in the East China sea and South China sea, Sci. China Tech. Sci. 55 (1) (2012) 163–173.
[7] A.M. Muzathik, W.B. Wan Nik, M.Z. Ibrahim, K.B. Samo, Wave energy potential of peninsular Malaysia, ARPN J. Eng. Appl. Sci. 5 (7) (2010) 11–23.
[8] A. Mirzaei, F. Tangang, L. Juneng, Wave energy potential along the east coast of Peninsular Malaysia, Energy 68 (2014) 722–734.
[9] G. Kim, W.M. Jeong, K.S. Lee, K. Jun, M.E. Lee, Offshore and nearshore wave energy assessment around the Korean Peninsula, Energy 36 (2011) 1460–1469.
[10] N. Guillou, G. Chapalain, Numerical modelling of nearshore wave energy resource in the Sea of Iroise, Renew. Energy 83 (2015) 942–953.
[11] S. Gallagher, R. Tiron, F. Dias, A long-term nearshore wave hindcast for Ireland: Atlantic and Irish Sea coasts (1979 -2012), Ocean. Dyn. 64 (2014) 1163–1180.
[12] S. Gallagher, R. Tiron, E. Whelan, E. Gleeson, F. Dias, R. McGrath, The nearshore wind and wave energy potential of Ireland: a high resolution assessment of availability and accessibility, Renew. Energy 88 (2016) 494–516.
[13] L. Liberti, A. Carillo, G. Sannino, Wave energy resource assessment in the Mediterranean, the Italian perspective, Renew. Energy 50 (2013) 938–949.
[14] A. Akpinar, M.I. Komurcu, Assessment of wave energy resource of the Black Sea based on 15-year numerical hindcast data, Appl. Energy 101 (2013) 502–512.
[15] L. Rusu, Assessment of the wave energy in the Black Sea based on a 15-year hindcast with data assimilation, Energies 8 (2015) 10370–10388.
[16] M.T. Pontes, R. Aguiar, H. Oliveira Pires, A nearshore wave energy atlas for Portugal, J. Offshore Mech. Arct. Eng. 127 (3) (2005) 249–255.
[17] J.E. Stopa, K.F. Cheung, Yileng Chen, Assessment of wave energy resources in Hawaii, Renew. Energy 36 (2) (2011) 554–567.
[18] M. Folley, T.J.T. Whittaker, Analysis of the nearshore wave energy resource, Renew. Energy 34 (7) (2009) 1709–1715.
[19] L. Hammar, J. Ehnberg, A. Mavume, S. Molander, Renewable ocean energy in the western Indian Ocean, Renew. Sustain. Energy Rev. 16 (2012) 4938–4950.
[20] V. Sanil Kumar, T.R. Anoop, Wave energy resource assessment for the Indian Shelf seas, Renew. Energ 76 (2015) 212–219.
[21] B. Kamranzad, A. Etemad-shahidi, V. Chegini, Assessment of energy variation in the Persian Gulf, Ocean. Eng. 70 (2013) 72–80.
[22] R.G. Quayle, M.J. Changery, Estimates of coastal deepwater wave energy potential for the world, in: Proceedings of Conference of Oceans, IEEE, Boston, MA, 1981, pp. 903–907.
[23] T. Ching-Piao, H. Ching-Her, H. Chien, C. Hao-Yuan, Study on the wave climate variation on the renewable energy assessment, Renew. Energy 38 (2012) 50–61.
[24] Zheng Chongwei, Zhuang Hui, Li Xin, Li XunQiang, Wind energy and wave energy resources assessment in the East China Sea and South China Sea, Sci. China 55 (1) (2012) 163–173.
[25] M.G. Hughes, A.D. Heap, National-scale wave energy resource assessment for Australia, Renew. Energy 9 (2010) 1783–1791.
[26] D.K. Ralston, H. Jiang, J.T. Farrar, Waves in the Red Sea: response to monsoonal and mountain gap winds, Cont. Shelf Res. 65 (2013) 1–13.
[27] S. Langodan, L. Cavaleri, Y. Viswanadhapalli, I. Hoteit, The Red Sea: a natural laboratory for wind and wave modelling, J. Phys. Oceanogr. 44 (2014) 3139–3159.
[28] Rasul NMA, Stewart ICF, Nawab ZA. Introduction to the Red sea: its origin, structure, and environment. In N.M.A. Rasul, I.C.F. Stewart (Eds.) The Red Sea the Formation, Morphology, Oceanography and Environment of a Young Ocean Basin, Springer Earth System Sciences, p 1 – 24. DOI 10.1007/978-3-662-45201-1_1.
[29] H.L. Tolman, User Manual and System Documentation of WAVEWATCH III Version 4.18, 2014, p. 151, http://dx.doi.org/10.3390/ijerph2006030011. NOAA/NWS/NCEP/MMAB Tech. Note.
[30] H.L. Tolman, B. Balasubramaniyan, L.D. Burroughs, D.V. Chalikov, Y.Y. Chao, H.S. Chen, V.M. Gerald, Development and implementation of wind generated ocean surface wave models at NCEP, Weather Forecast. 17 (2002) 311–333.
[31] G.J. Komen, L. Cavaleri, M. Donelan, K. Hasselmann, S. Hasselmann, P.A.E.M. Janssen, Dynamics and Modelling of Ocean Waves, Cambridge University Press, Cambridge, 1994, 532 pp.
[32] H.L. Tolman, D. Chalikov, Source terms in a third-generation wind wave model, J. Phys. Oceanogr. 26 (1996) 2497–2518.
[33] J.R. Bidlot, P. Janssen, S. Abdalla, A Revised Formulation of Ocean Wave Dissipation and its Model Impact, ECMWF Tech. Rep. Memo, Reading, 2007.
[34] F. Ardhuin, E. Rogers, A.V. Babanin, J.F. Filipot, R. Magne, A. Roland, A. van der Westhuysen, P. Queffeulou, J.M. Lefevre, L. Aouf, F. Collard, Semiempirical dissipation source functions for ocean waves. Part I: definition, calibration, and validation, J. Phys. Oceanogr. 40 (2010) 1917–1941.
[35] S. Zieger, A.V. Babanin, I.R. Young, Changes in ocean surface wind with a focus on trends in regional and monthly mean values, Deep. Res. Part I Oceanogr. Res. Pap. 86 (2014) 56–67.
[36] J.J. Becker, D.T. Sandwell, W.H.F. Smith, J. Braud, B. Binder, J. Depner, D. Fabre, J. Factor, S. Ingalls, S.H. Kim, R. Ladner, K. Marks, S. Nelson, S. Pharaoh, A. Trimmer, A. Von Rosenberg, G. Wallace, P. Weatherall, Global bathymetry and elevation data at 30 arc seconds resolution: SRTM30_PLUS, Mar. Geod. 32 (4) (2009) 355–371.
[37] A. Chawla, D.M. Spindler, H.L. Tolman, Validation of a thirty year wave hindcast using the Climate Forecast System Reanalysis winds, Ocean. Model. 70 (2013) 189–206.
[38] X. Bao, F. Zhang, Evaluation of NCEP–CFSR, NCEP–NCAR, ERA-Interim, and ERA-40 reanalysis datasets against independent sounding observations over the Tibetan Plateau, J. Clim. 26 (2013) 206–214.
[39] J.E. Stopa, K.F. Cheung, Intercomparison of wind and wave data from the ECMWF reanalysis interim and the NCEP climate forecast system reanalysis, Ocean. Model. 75 (2014) 65–83.
[40] E. Sharp, P. Dodds, M. Barret, C. Spataru, Evaluating the accuracy of CFSR reanalysis hourly wind speed forecasts for the UK, using in situ measurements and geographical information, Renew. Energy 77 (2015) 527–538.
[41] S.V. Samiksha, P. Vethamony, V.M. Aboobacker, R. Rashmi, Propagation of Atlantic ocean swells in the north Indian Ocean: a case study, Nat. Hazards Earth Syst. Sci. 12 (2012) 3605–3615.
[42] R. Scharroo, E.W. Leuliette, J.L. Lillibridge, D. Byrne, M.C. Naeije, G.T. Mitchum, RADS: consistent multi-mission products, in: Proc. of the Symposium on 20 Years of Progress in Radar Altimetry, Venice, 20-28 September 2012, Eur. Space Agency Spec. Publ., 2013. ESA SP-710, p. 4 pp.
[43] I.R. Young, J. Vinoth, S. Zieger, A.V. Babanin, Investigation of trends in extreme value wave height and wind speed, J. Geophys. Res. 117 (2012). C00J06, 1–13.
[44] P.K. Bhaskaran, N. Gupta, M.K. Dash, Wind-wave climate projections for the Indian Ocean from satellite observations, J. Mar. Sci. Res. Dev. (2014), http://dx.doi.org/10.4172/2155-9910.S11-005. **S11**: Article number: 005.
[45] G.A. Meehl, T.F. Stocker, W.D. Collins, P. Friedlingstein, A.T. Gaye, J.M. Gregory, A. Kitoh, R. Knutti, J.M. Murphy, A. Noda, S.C.B. Raper, I.G. Watterson, A.J. Weaver, Z.C. Zhao, Global climate projections, in: S. Solomon, D. Qin, M. Manning, Z. Chen, M. Marquis, K.B. Averyt, M. Tignor, H.L. Miller (Eds.), Climate Change 2007: the Physical Science Basis. Contribution of Working Group I to the Fourth Assessment Report of the Intergovernmental Panel on Climate Change, Cambridge University Press, Cambridge, United Kingdom and New York, NY, USA, 2007.

Please cite this article in press as: V.M. Aboobacker, et al., Wave energy resource assessment for Red Sea, Renewable Energy (2016), http://dx.doi.org/10.1016/j.renene.2016.09.073